Nanoscale

Accepted Manuscript

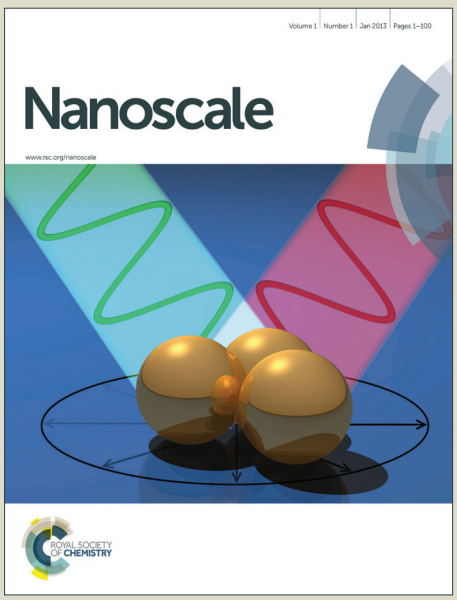

ROYAL SOCIETY OF CHEMISTRY

www.rsc.org/nanoscale

Nanoscale

RSCPublishing

COMMUNICATION

Graphene controlled H- and J-stacking of perylene dye into highly stable supramolecular nanostructures for enhanced photocurrent generation†

Cite this: DOI: 10.1039/x0xx00000x

Received 00th April 2014,
Accepted 00th May 2014

DOI: 10.1039/x0xx00000x

www.rsc.org/

Shiyu Gan[a,b], Lijie Zhong[a,c], Christian Engelbrekt[b], Jingdong Zhang[b], Dongxue Han[a], Jens Ulstrup[b], Qijin Chi*[b] and Li Niu*[a]

We report a new method for controlling H- and J-stacking in supramolecular self-assembly. Graphene nanosheets act as structure inducers to direct the self-assembly of a versatile organic dye, perylene into two distinct types of functional nanostructures, i.e. one-dimensional nanotubes via J-stacking and two-dimensional branched nanobuds through H-stacking. Graphene integrated supramolecular nanocomposites are highly stable and show significant enhancement of photocurrent generations in the two configurations of photosensing devices, i.e. solid-state optoelectronic construct and liquid-junction solar cell.

Supramolecular chemistry has enabled creating complex ensembles with functionalities beyond those of the individual molecules.[1] Perylene bisimides (PBIs), known as a family of organic dyes, are among the most versatile building blocks for development of supramolecular nanostructures. Based on the supramolecular chemistry of PBIs studied intensively by Würthner[2] and Müllen[3] groups in particular, PBI based supramolecular nanostructures show a broad spectrum of promising applications in organic nanodevices[4], artificial light-harvesting systems[5] and biomimetic functional modules.[6] PBIs have a core structure composed of five condensed benzene rings that drive intermolecular self-assembly via π-π stacking. PBIs and other π-conjugated organic dye molecules favor two major types of molecular stacking modes, namely H- and J-stacking[2b]. H-stacking is a "face-to-face" molecular connection to form supramolecular aggregates and could result in a blue-shift in the absorption bands (also called hypsochromical (H-) shift) compared to the monomer form. J-stacking represents a slipped molecular self-assembly with red-shifted aggregation absorptions. About 80 years ago, Scheibe and Jelley first observed an interesting spectroscopic absorption behavior of a pseudoisocyanine (PIC) dye in water and ethanol[7, 8]. Scheibe found a sharp peak at the long wavelength upon injecting water to a PIC monomer containing ethanol solution. He lately interpreted this red-shifted behavior as a consequence of molecular polymerization leading to a desolvation or a "vicinity effect" (which could be considered as the rudiment of the supramolecular concept)[7]. Meanwhile, Jelley observed an aggregation process of PIC dye in ethanol upon addition of nonpolar solvents or concentrated salt aqueous solutions (e.g. 5 M NaCl)[8]. Owing to their pioneering discoveries, this type of aggregation behavior is often termed as J-aggregation.

To date, the widely used strategy for controlling the H and J-stacking is structural modifications of monomers via synthetic chemistry[9]. For example, Würthner and coworkers reported that grafting methyl groups at the alkyl side chains of a PBI derivative can hamper its originally preferable H-stacking because of the steric hindrance and instead favor J-stacking[9a] Two PBI derivatives synthesized by Li and coworkers have only one benzene difference at side chains but show very different stacking interactions.[9d] Yagai et. al. reported a strategy to control H- to J-stacking by introducing a ligand (i.e. cyanurate) with a hydrogen-bond-directed interaction with target PBI derivatives[10]. They also found that the concentration ratio of PBI to ligand plays a crucial role in the formation of supramolecular aggregates. These two methods arguably represent current main strategies for controlling H- and J-stacking self-assembly. However, cost-effective and facile approaches are still lacking. In addition, integration of functional supramolecular nanostructures with a solid support is highly desirable for their applications in nanoelectronics, electrochemical catalysis and energy technology. However, supramolecular self-assembly is favored predominantly in homogeneous solution, so that the non-destructive transfer of sophisticated supramolecular nanostructures from a solution onto a solid substrate remains a challenge.

As a "wonder material", graphene has generated intensive interest in physics, chemistry and materials science within the last decade.[11] Among several methods developed for preparation of graphene nanosheets, wet-chemical methods enable low-cost production and facile functionalization of graphene sheets by solution processing.[12] To distinguish from pristine graphene prepared for example by mechanical exfoliation and chemical vapor deposition, chemical graphenes are here broadly referred to as graphene oxide (GO), reduced graphene oxide (RGO) and their derivatives. While pristine graphene is water insoluble and chemically inert, chemical graphenes are chemically tunable. GO and RGO have shown versatile advantages by acting as soluble soft supports to deposit various functional nanomaterials for materials chemistry[13] and to load enzymes[14] or to deliver drugs[15] for nanomedicine. In addition, a few reports have focused on their structural scaffold roles by exploiting their intrinsic two-dimensional (2D) planar and structural imperfection features. For example, GO acts as an atomic scaffold for directed synthesis of hexagonal closed-

packed gold nanosheets[16]. GO and RGO has been also used in preparation of nickel hydroxide nanostructures for supercapacitors.[17]

Inspired by these recent studies, herein, for the first time we exploit the intrinsic structures of GO and RGO nanosheets to direct and control the H- and J-supramolecular self-assembly of a representative of PBI organic dyes, perylene (Py) into specific nanostructures. In addition to fundamental investigations on controlled supramolecular self-assembly and structural characteristics, we have also explored two proof-of-concept photosensitive applications in optoelectronic devices and liquid-junction solar cells. Compared to pure GO, RGO and Py, GO/RGO-Py nanocomposites show significant enhancement of photocurrent generation in both liquid- and solid-state devices.

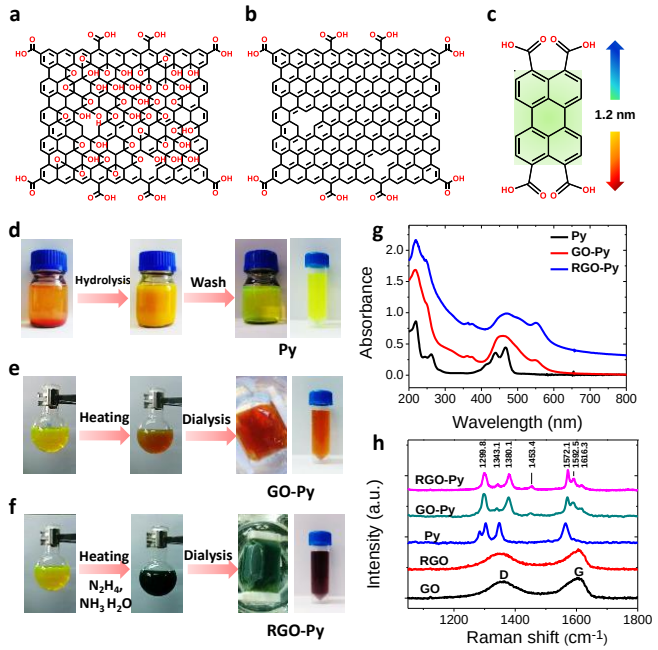

Fig. 1 Wet-chemical preparation and spectroscopic analysis of GO-Py and RGO-Py. (a-c) Chemical structures of GO, RGO and Py. (d) Hydrolysis of PTCDA into Py with liberated carboxylic groups. (e) Heat-assisted preparation of GO-Py nanostructures at 95 °C and purification by dialysis. (f) Heat-assisted preparation of RGO-Py nanostructures at 95 °C in the presence of reducing reagent N_2H_4 and purification by dialysis. (g) UV-vis spectra of Py (5.6 μg ml^{-1}) (black curve), GO-Py (26.2 μg ml^{-1}) (red curve) and RGO-Py (17.5 μg ml^{-1}) (blue curve) dispersed in pure water. (h) Raman spectra of GO, RGO, pure Py, GO-Py and RGO-Py films deposited on glass substrates. The spectra were recorded using 514.5 nm as an excitation wavelength, and their intensity are normalized for comparison.

The chemical structures of GO, RGO and Py are schematically illustrated in Fig. 1a-c, respectively. Single-layered GO and RGO were synthesized by our previous procedure[18] and characterized systematically by atomic force microscopy (AFM) and spectrophotometry (Fig. S1, ESI†). Py was obtained by hydrolysis of the anhydride 3, 4, 9, 10-perylenetetracarboxylic dianhydride (PTCDA) in NaOH, followed by dialysis and filtration for purification (Fig. 1d). The as-prepared Py is water soluble with yellowish green color (Fig. 1d). Spectrophotometry offers a simple but effective means to characterize chemical states of Py in solution. UV-vis absorption bands of pure Py aqueous solution originating from $S_0 \rightarrow S_1$ electronic transitions appear in the range of 350-500 nm, with absorbance peaks at 415, 439 and 467 nm attributed to 0→2, 0→1 and 0→0 transitions,[19] respectively (Fig. 1g, black line, and Fig. S2, ESI†). To address the structural inducing effects of GO and RGO on supramolecular self-assembly, we first tested whether or not Py alone would self-assemble into aggregated structures. No shift in peak positions for different concentrations of Py (Fig. S2, ESI†) and the constant $A^{0\rightarrow0}/A^{0\rightarrow1}$ ratio at 1.2 are clear indications that Py monomers are stable in their isolated form under our experimental conditions.[19]

Heat-assisted wet-chemistry was used to promote the formation of graphene-supported supramolecular nanostructures. In the presence of GO, the Py solution rapidly turned from yellowish green to red upon heating (Fig. 1e). Control experiments, with no GO included in the reaction solution, showed neither color change nor spectral shift (Fig. S3, ESI†). The simultaneous assembly of Py supramolecular nanostructures and chemical reduction of GO occurred upon the additional presence of the reducing agent hydrazine, leading to the formation of RGO-Py ensembles (Fig. 1f). Both GO-Py and RGO-Py ensembles are well dispersed in water and highly stable, as evidenced by no aggregation detected and identical UV-vis spectra recorded after one-year storage (Fig. S5, ESI†).

We characterized the nanostructures first by qualitative analysis using spectrophotometry and Raman spectroscopy, followed by structural imaging using high-resolution microscopies. From the UV-vis spectra (Fig. 1g), three major changes upon Py self-assembly on GO are: (1) the three distinct bands for free Py reduced to two bands with the 0→2 and 0→1 bands merging into a single band, (2) significant red- shift (82 nm for 0→0 and 44 nm for 0→2) and band broadening, and (3) the $A^{0\rightarrow0}/A^{0\rightarrow1}$ ratio reduced from 1.2 to 0.57 (Fig. S4, ESI†). Similar changes are observed for the case of RGO-Py (Fig. 1g, blue line). Raman spectra offer further support for formation of Py supramolecular nanostructures on GO and RGO (Fig. 1h and Table S1, ESI†). GO and RGO are characterized by D and G bands at 1357.0/1605.1 cm^{-1} for GO and at 1347.5/1607.6 cm^{-1} for RGO[12a]. After integrating Py supramolecular nanostructures, several new peaks emerged in the D and G band regions (Fig. 1h), and the D and G bands are significantly shifted (Table S1, ESI†). Compared to the Raman spectra of free Py monomer supramolecular assembly has invoked significant vibrational changes as well, indicated by the disappearance of the B_{3g} vibration mode at 1347.4 cm^{-1} (δC-C, C-C bending) and by the emergence of three A_g vibrations at 1379.5, 1451.6 and 1588.9 cm^{-1} (on GO) and at 1380.1 cm^{-1}, 1453.4 and 1592.5 cm^{-1} (on RGO). These observations suggest that strong interactions between Py and GO (or RGO) accompany the formation of integrated nanostructures.

Transmission electron microscopy (TEM) and AFM were used to reveal the structural features of GO-Py and RGO-Py ensembles. TEM and AFM images show that Py was self-assembled into nanotubular structures on GO (Fig. 2a-2d and Figs. S6 and S7, ESI†). Py nanotubes have a diameter of 20 nm and a wall thickness 1.2-1.4 nm, as estimated from high-resolution TEM (HRTEM) images (Fig. 2c and Fig. S6d-6i, ESI†). The thickness accords with the lateral size of Py molecules (about 1.2 nm, Fig. 1c). These structural features are also seen by AFM (Fig. 2d and Fig. S7). In contrast, the Py supramolecular structure is branched, along the wrinkles of RGO sheet planes with an apparent shape like a tree-bud (Fig. 2e-2f), hereafter termed "nanobud" for ease of the description. HRTEM images show that the nanobuds are solid with a diameter of 10-20 nm (Fig. 2g and Fig. S8, ESI†). AFM discloses similar structural features and estimate their thickness as 5-6 nm (Fig. 2h and Fig. S9b-9d, ESI†), equivalent to the approximate size of 10-20 Py molecules assembled in vertical direction with respect to the RGO planes. Fast Fourier transform (FFT) and selected area electron diffraction (SAED) analysis confirm that GO and RGO maintain their intrinsic carbon plane structures after the non-covalent functionalization by Py molecules (Fig. S10, along with the detailed discussion provided in ESI†).

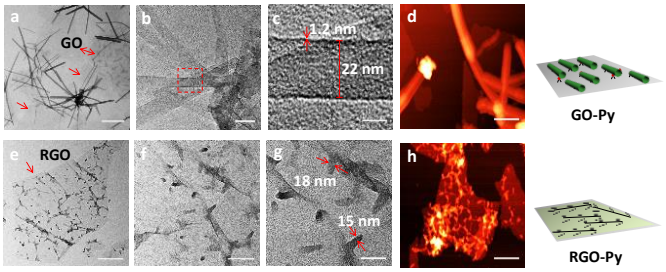

Fig. 2 Microscopic analysis of morphology and structures of GO-Py and RGO-Py. (a, b) TEM images of GO-Py nanostructures. (c) A HRTEM image obtained from the area marked in (b). (d) An AFM image of GO-Py on mica. (e, f) TEM images of RGO-Py nanostructures. (g) A HRTEM image obtained from the area in (f). (h) An AFM image of RGO-Py on mica. Scale bars: (a-b) 400 nm, 50 nm and 10 nm; (e-g) 300 nm, 100 nm and 50 nm; (d) and (h) 300 nm, respectively. The insets (right): schematic illustration of structures for Py nanotubes on GO and Py nanobuds on RGO.

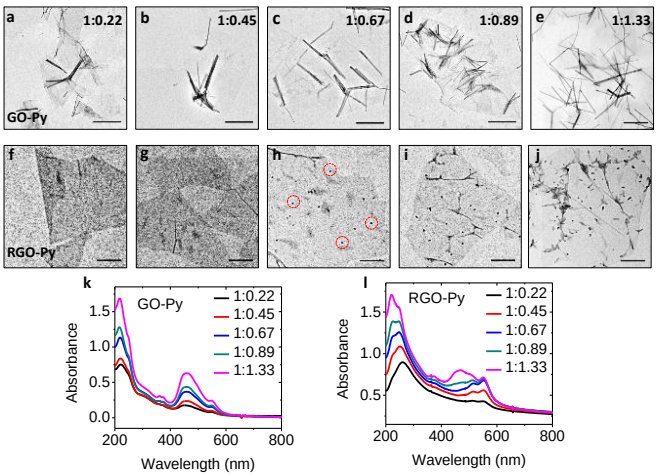

Fig. 3 Concentration-dependent self-assembly of Py on GO and RGO. (a-e) and (f-j) representative TEM images of Py growth on GO (a-e) and RGO (f-j) at different concentrations controlled by the initial mass ratios of GO to Py ranging from 1: 0.22 to 1: 1.33. The red circles marked in (h) represent small size but visible Py nanostructures grown RGO when the mass ratio reaching 1:0.67. (k, l), Corresponding UV-vis absorption spectra for GO-Py (k) and RGO-Py (l) samples obtained at different ratios. Scale bars: (a-e) 500 nm and (f-j) 200 nm.

To illustrate the formation process of Py supramolecular nanostructures on graphene sheets, the effect of Py initial concentration was examined. For Py self-assembly on GO the density of nanotubes increases with increasing Py concentration, but their morphology remained unchanged (Fig. 3a-3e). UV-vis spectra confirm a gradual stepwise increase in intensity, but apparently no peak shift (Fig. 3k). In the case of Py on RGO, the Py concentration shows a more profound effect. At low concentrations, Py nanostructures are too small to be imaged by TEM (Fig. 3f and 3g). However, the UV-vis spectra (Fig. 3l) and AFM images (Fig. S9, ESI†) suggest that Py was adsorbed on RGO. With increasing Py concentration further, supramolecular nanostructures became TEM visible (Fig. 3h) and grew into nanobuds (Fig. 3i-3j). A blue-shift of the $A^{0\rightarrow2}$ band is observed, when the mass ratio reached 1:1.33 (Fig. 3l). These observations suggest that Py concentration is a crucial controlling factor. While Py enables forming nanotubes on GO at low concentrations, the formation of Py nanobuds on RGO requires a threshold concentration with the mass ratio of GO to Py at 1:0.67.

Host-guest interaction is arguably the most fundamental principles of supramolecular chemistry. A conceptual analogue might apply to the present case, by considering GO or/and RGO as a host-like support and Py as a guest molecule. The different intrinsic structure between GO and RGO induces different "host-guest" interactions, leading to the formation of two distinct types of Py supramolecular nanostructures. Based on such considerations and our experimental observations, we propose the possible formation mechanisms illustrated schematically in Fig. 4. Individual GO nanosheets are of rich oxygen containing groups (C:O ≈ 2:1, Fig. S11, ESI†) which contain hydroxyl and epoxy groups[20] (Fig. 1a). In contrast, RGO is a product of chemical reduction of GO with oxygen containing groups removed mostly and the sp^2 planes restored largely (C: O ≈ 10:1, Fig. S11, ESI†). As illustrated, PBIs favor two major types of molecular self-assembly, i.e. J-stacking and H-stacking aggregations.[2]

GO nanosheets induce J-stacking molecular self-assembly of Py to yield nanotubular structures (Fig. 4a). Supramolecular self-assembly is most likely initiated by hydrogen-bonding between Py molecules and oxidized hydrophilic regions on the GO plane. The adsorbed Py molecules serve as a structural inducer facilitating J-type intermolecular interactions of Py molecules coming from the solution. This self-assembly process is consistent with the experimental observations: (1) the thickness of the Py nanotube walls is around 1.2-1.4 nm (Fig. 2c), corresponding to the single-layer lateral dimension of Py molecules (Fig. 1c). (2) Py nanotubes form even at low Py concentrations (Fig. 3a-3c), as expected from J-stacking self-assembly. (3) In terms of nanotube density, a monolayer (or sub-monolayer) rather than multilayers on GO was consistently observed even at high concentrations of Py monomers (Fig. 3d-3e). In the case of RGO, H-stacking molecular self-assembly leads to the formation of branched and tree-like structures consisting of Py nanobuds (Fig. 4b). Py is structurally like a molecule-size RGO nanosheet (Fig. 1b and 1c), which would facilitate chemically compatible π-π stacking interaction between Py and RGO. As illustrated in Fig. 4b, Py molecules are first absorbed on the RGO plane via π-π stacking to form a (sub)monolayer. Then, small nanobuds are formed by local H-stacking. Finally, these small nanobuds grow along both the horizontal and vertical directions into a tree-like network nanostructure by expanding H-stacking aggregation. Our experimental observations that support the proposed mechanism include: (1) the formation of nanobuds requires a threshold concentration (Fig. 3f-3j). (2) Blue-shifted UV-vis spectra are clearly observed and become more profound with increasing Py concentration (Fig. 3l), which is consistent with the effects of Py concentration on H-stacking self-assembly[9a.] (3) The 10-20 nm width and 5-6 nm height of nanobuds reflect 10-20 molecules self-assembled in horizontal and vertical directions, respectively (Fig. 2e-2h and Figs. S8 and S9, ESI†) (for more supramolecular mechanisms, see supplementary discussions in supporting information).

Following studies on nanostructure formation, high-resolution structural characterization and controlled supramolecular self-assembly described above, herein, we tested a proof-of-concept functional application of photocurrent generations by GO/RGO-Py materials, on the basis of prominently red-shifted Py absorption bands shown in Fig. 1g. Two types of photocurrent configurations were proposed and tested, i.e., optoelectronic devices in air (solid state) and liquid-junction solar cells in solution environments (liquid phase). Using a home-made prototype optoelectronic device, typical current (*I*)-voltage (*V*) characteristics indicate that the RGO-Py film

is photoelectrically sensitive (Fig. 5a), whereas no signal was observed for pure Py film and little response from GO-Py film owing to their low electric conductivity (Fig. S12, ESI†). Upon successive on-off light switching, RGO-Py film displays reversible conductance switching with an ON-OFF ratio of ca. 5 (Fig. 5b, red line), which is more than twice enhancement compared to pure RGO film (Fig. 5b, black line). Such performance is close to or even better than those reported for nanostructured inorganic semiconductor materials, such as ZnO[21] and $NiCo_2O_4$ nanofilms[22] for photodetector applications.

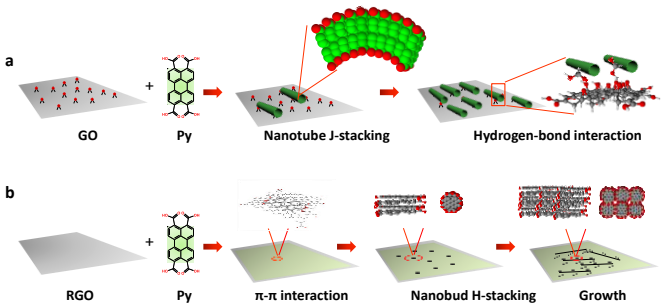

Fig. 4 Schematic illustration of proposed mechanisms. (a) Supramolecular self-assembly of Py on GO, where J-stacking type self-assembly is initiated by hydrogen-bonding interactions between Py molecules and oxygen-containing groups on the GO plane, leading to growth into nanotubes. (b) Supramolecular self-assembly of Py on RGO, where Py molecules are first absorbed on the RGO plane via π-π stacking interactions (see the amplified scheme), followed by the formation of small-size nanobuds through local H-stacking interactions (see the amplified schemes, side and top views). Finally, these small nanobuds grow along the horizontal and vertical directions into tree-like structures.

Liquid-junction solar cells based on a solution-phase photocurrent generation could become a new-generation and efficient energy conversion setup for utilization of solar energy.[23] Fig. 5c shows a typical photoelectrochemical cell, in which LiI and I_2 were used as electrolyte and redox species, and GO/RGO-Py modified ITO electrodes were used as light-sensitive working electrodes. While pure GO and RGO generate negligible photocurrents (black lines, Fig. 5d), GO/RGO-Py show remarkably enhanced photocurrent generations. Their photocurrents are 2 μA cm^{-2} and 8 μA cm^{-2} respectively (red lines, Fig. 5d), which are 5-20 times the photocurrent generated by pure Py molecule (Fig. S13, ESI†). Moreover, it should be noted that we found in experiments GO-Py and RGO-Py were easily formed into uniform films covered on ITO by drop-casting or spin-coating but not for pure Py molecules. Such photocurrent performances approach to the recently reported photo-electrochemical studies of RGO-porphyrin nanohybrids[24] but relative low cost of our light-sensitive materials (Py) may be preponderant in future GO/RGO based liquid-junction solar cell applications.

The exact chemistry and physics behind these photocurrent enhancements for the optoelectnonic device and liquid-junction solar cell are not fully understood, but it could be apparently attributed to the enhanced absorptions by the red-shifted Py nanostructures (Fig. 1g). The presence of Py supramolecular nanostructures and π delocalization further enables GO/RGO-Py to absorb light extending to visible spectral regions. Such characteristics could promote the solar energy utilization. In addition, note that the functional mechanisms for two types of applications are quite different. The optoelectronic device in air environment is based on the resistant variation upon light illumination. That is why little photocurrent-response was observed for pure GO-Py optoelectronic device due to its high resistance (Fig. S12, ESI†). However, such resistant effect is not significant in solution-phase solar cell. For example, GO-Py also shows a prominent photocurrent (Fig. 5d, top). Further work will be devoted to studying the detailed photocurrent response mechanisms.

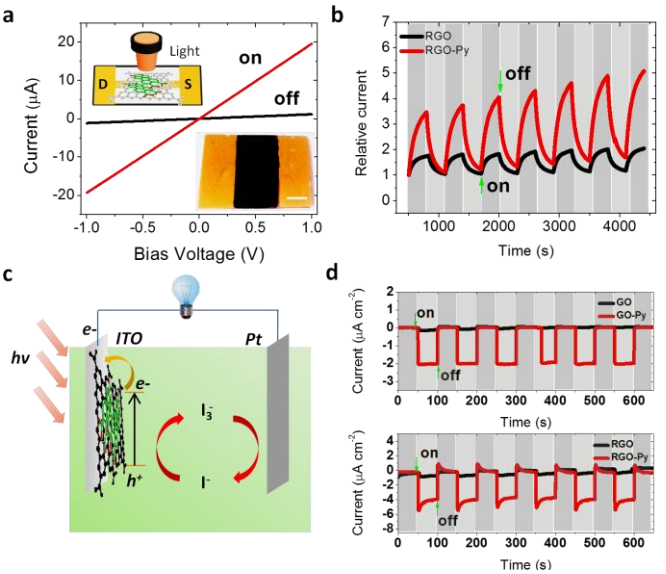

Fig. 5 Photocurrent responses of GO-Py and RGO-Py. (a) *I-V* curves of RGO-Py films under light off (black curve) and upon light illumination (red curve). The insets are a schematic illustration of home-made devices (top) and its digital photo (RGO-Py, bottom), scale bar 5 mm. Voltage scanning rate: 100 mV s^{-1}. (b) Transient photocurrent responses from RGO-Py and RGO based devices, in which the current is normalized to show the ON-OFF ratio. The bias voltage is +1 V. (c) A schematic illustration of solution phase photocurrent generation electrochemical setup. The electrolyte is N_2 saturated 0.5 M LiI and 0.01 M I_2 in acetonitrile. GO/RGO-Py modified ITO and Pt electrodes were used as working and counter electrodes, respectively. (d) Photocurrent responses of GO/ITO and GO-Py/ITO electrodes (top), RGO/ITO and RGO-Py/ITO electrodes (bottom) at open circuit potentials. The white light (λ > 400 nm and input power 150 mW cm^{-2}) was used as a light source for the photocurrent generation experiments.

Functionalization of graphene by photoactive molecules is one of the most devoted subjects in graphene chemistry. Various organic photoactive molecules have been proposed, among which two types of typical π-conjugated building blocks, i.e. porphyrins[25] and PBI dyes[26] have gained intensive attention. Guldi and coworkers have reported a series of porphyrin derivatives to functionalize graphene through non-covalent[25c] and covalent[25d] approaches. Their work demonstrates that graphene can promote the charge separation and reduce the recombination of photoactive porphyrin molecules based on the time-resolved spectroscopic measurements. On the other hand, PBI dyes exhibit strong π-π interactions with graphene owing to their delocalized π-structure with five-connected benzene rings. Hirsch and coworkers have used various PBI derivatives for direct exfoliation of graphite in water[26b] or organic solvents[26c] into soluble and stable graphene nanosheets. The electronic communication or energy transfer between graphene and PBI has been demonstrated by typical spectroscopic characterizations including absorption, Raman and fluorescence spectra[26]. In the present work, we have explored their interactions by a reversal approach. We used a representative PBI unit (i.e. Py) and two water-soluble graphene derivatives (i.e. GO and RGO) to demonstrate the distinctive structural inductions. Our spectral observations, for example red-shifted Py absorption and superimposed Py Raman bands, are similar to those for PBI dyes functionalized on carbon nanotube or graphene nanosheets[26c, d]. This confirms that strong electronic interactions between GO/RGO and Py occurred.

As a final note, supramolecular self-assembly is favored predominantly in homogeneous solution by injection of a so-called

"poor" solvent into a monomer-containing "good" solvent. Integration of supramolecular nanostructures with a solid support is highly desirable for applications in nanoelectronics and electrochemical catalysis, but the non-destructive transfer of sophisticated supramolecular nanostructures from a solution onto a solid substrate remains a challenge. Recently, Rabe and coworkers immobilize individual cyanine dye nanotubes on solid substrates by a drop-flow technique without affecting their nanostructures[27]. In the present work, GO and RGO are used as solution dispersible soft substrates. Our approach could open an alternatively new strategy to directly induce the supramolecular formation and to simultaneously immobilize supramolecular nanostructures onto a solid conductive support with no need of the challenging transfer procedure.

Conclusions

In summary, a new strategy by exploiting the intrinsic structure features of GO and RGO was demonstrated to control the J- and H-stacking self-assembly of Py dye, leading to the formation of 1D nanotubes (J-stacking) and 2D branched nanobuds (H-stacking). Py is structurally simple among PBI family, but it represents the core structures of all PBI molecules. The present work is focused only on Py, but the method demonstrated is expected to be applicable for directed supramolecular self-assembly of other PBI molecules. Further research on detailed mechanisms of controlled supramolecular self-assembly induced by chemical graphenes and fabrications of sophisticated optoelectronic devices (for example, GO/RGO-Py based optoelectronic devices using single nanosheet instead of the thin films in the present work), and systematical studies on liquid-junction solar cells including photo-to-electron efficiency and photovoltage performance are desirable and anticipated in the ongoing efforts.

Acknowledgements

We are grateful for the financial support from the National Science Foundation of China (No. 21225524, No.21175130, No.21105096 and No.21205112), the Department of Science and Technology of Jilin Province (No.20120308 and No.201215091), the Danish Research Council for Technology and Product Science (Project No. 12-127447), the Lundbeck Foundation (Grant No. R49-A5331), and the European Framework Program-Marie Curie Actions under the ELECTRONANOMAT Project (Grant No. PIRSES-GA-2012-318990). S.G. acknowledges the Universities Denmark for a guest PhD studentship. J.Z. and L.N. acknowledge the Otto Mønsteds Fond for a visiting professorship. We thank Dr Wei Song for the assistance in the Raman spectroscopy experiments and Dr. Mohsin Javed for the valuable discussion.

Notes and references

[a] *State Key Laboratory of Electroanalytical Chemistry, c/o Engineering Laboratory for Modern Analytical Techniques, Changchun Institute of Applied Chemistry, Chinese Academy of Sciences, Changchun 130022, and University of Chinese Academy of Sciences, Beijing, 100049, P. R. China. E-mail: lniu@ciac.ac.cn*
[b] *Department of Chemistry, Technical University of Denmark, Kemitorvet, Building 207, DK-2800 Kongens Lyngby, Denmark. E-mail: cq@kemi.dtu.dk*
[c] *Present address: Department of Energy Conversion and Storage, Technical University of Denmark, Kemitorvet, Building 207, DK-2800 Kongens Lyngby, Denmark.*
† Electronic Supplementary Information (ESI) available: Material and methods, spectroscopic data, AFM and TEM images, materials functional tests and supplementary discussions. See DOI: 10.1039/b000000x/

1. (a) J. M. Lehn, *Supramolecular chemistry: concepts and perspectives.* 1995, Willey VCH, Germany; (b) R. Chakrabarty, P. S. Mukherjee and P. J. Stang, *Chem. Rev.*, 2011, **111**, 6810. (c) H. J. Schneider, *Applications of supramolecular chemistry.* 2012, CRC Press; (d) E. Busseron, Y. Ruff, E. Moulin and N. Giuseppone, *Nanoscale*, 2013, **5**, 7098.
2. (a) Z. Chen, A. Lohr, C. R. Saha-Moeller and F. Würthner, *Chem. Soc. Rev.*, 2009, **38**, 564; (b) F. Würthner, T. E. Kaiser and C. R. Saha-Moeller, *Angew. Chem. Int. Ed.*, 2011, **50**, 3376; (c) M. M. Safont-Sempere, G. Fernandez and F. Würthner, *Chem. Rev.*, 2011, **111**, 5784; (d) D. Görl, X. Zhang and F. Würthner, *Angew. Chem. Int. Ed.*, 2012, **51**, 6328.
3. (a) B. Schmaltz, T. Weil and K. Müllen, *Adv. Mater.*, 2009, **21**, 1067; (b) T. Weil, T. Vosch, J. Hofkens, K. Peneva and K. Müllen, *Angew. Chem. Int. Ed.*, 2010, **49**, 9068; (c) L. Chen, C. Li and K. Müllen, *J. Mater. Chem. C*, 2014, **2**, 1938.
4. (a) C. Li and H. Wonneberger, *Adv. Mater.*, 2012, **24**, 613; (b) T. M. Figueira-Duarte and K. Müllen, *Chem. Rev.*, 2011, **111**, 7260.
5. (a) P. D. Frischmann, K. Mahata and F. Würthner, *Chem. Soc. Rev.*, 2013, **42**, 1847.
6. X. Zhang, S. Rehm, M. M. Safont-Sempere and F. Würthner, *Nat. Chem.*, 2009, **1**, 623.
7. (a) G. Scheibe and A. Rivas, *Angew. Chem.*, 1936, **49**, 0443; (b) G. Scheibe, *Angew. Chem.,* 1937, **50**, 0212-0219; (c) G. Scheibe, L. Kandler and H. Ecker, *Naturwissenschaften*, 1937, **25**, 75.
8. (a) E. E. Jelley, *Nature*, 1936, **138,** 1009; (b) E. E. Jelley, *Nature*, 1937, **139**, 631.
9. (a) S. Ghosh, X.-Q. Li, V. Stepanenko and F. Würthner, *Chem. Eur. J.*, 2008, **14**, 11343; (b) T. E. Kaiser, V. Stepanenko and F. Würthner, *J. Am. Chem. Soc.*, 2009, **131**, 6719; (c) B. Jancy and S. K. Asha, *Chem. Mater.*, 2008, **20**, 169; (d) H. Wu, L. Xue, Y. Shi, Y. Chen and X. Li, *Langmuir*, 2011, **27**, 3074.
10. S. Yagai, T. Seki, T. Karatsu, A. Kitamura and F. Würthner, *Angew. Chem. Int. Ed.*, 2008, **47**, 3367.
11. (a) A. K. Geim, *Science*, 2009, **324**, 1530; (b) C. N. R. Rao, A. K. Sood, K. S. Subrahmanyam and A. Govindaraj, *Angew. Chem. Int. Ed.*, 2009, **48**, 7752.
12. (a) S. Stankovich, D. A. Dikin, R. D. Piner, K. A. Kohlhaas, A. Kleinhammes, Y. Jia, Y. Wu, S. T. Nguyen and R. S. Ruoff, *Carbon*, 2007, **45**, 1558.
13. (a) H. Yang, F. Li, C. Shan, D. Han, Q. Zhang, L. Niu and A. Ivaska, *J. Mater. Chem.*, 2009, **19**, 4632; (b) F. Li, H. Yang, C. Shan, Q. Zhang, D. Han and A. Ivaska, L. Niu, *J. Mater. Chem.*, 2009, **19**, 4022; (c) X. Huang, X. Qi, F. Boey and H. Zhang, *Chem. Soc. Rev.*, 2012, **41**, 666; (d) X. Huang, Z. Yin, S. Wu, X. Qi, Q. He, Q. Zhang, Q. Yan, F. Boey and H. Zhang, *Small*, 2011, **7**, 1876; (e) C. Tan, X. Huang and H. Zhang, *Mater. Today*, 2013, **16**, 29; (f) X. Qi, C. Tan, J. Wei and H. Zhang, *Nanoscale*, 2013, **5**, 1440.
14. (a) C. Shan, H. Yang, J. Song, D. Han, A. Ivaska and L. Niu, *Anal. Chem.*, 2009, **81**, 2378; (b) T. Kuila, S. Bose, P. Khanra, A. K. Mishra, N. H. Kim and J. H. Lee, *Biosens. Bioelectron.*, 2011, **26**, 4637.
15. V. Biju, *Chem. Soc. Rev.*, 2014, **43**, 744.
16. (a) X. Huang, S. Li, Y. Huang, S. Wu, X. Zhou, S. Li, C. L. Gan, F. Boey, C. A. Mirkin and H. Zhang, *Nat. Commun*., 2011, **2**, 292 doi:10.1038/ncomms1291; (b) X. Huang, S. Li, S. Wu, Y. Huang, F. Boey, C. L. Gan and H. Zhang, *Adv. Mater.*, 2012, **24**, 979; (c) X. Huang, H. Li, S. Li, S. Wu, F. Boey, J. Ma and H. Zhang, *Angew. Chem. Int. Ed.*, 2011, 50, 12245.
17. (a) H. Wang, J. T. Robinson, G. Diankov and H. Dai, *J. Am. Chem. Soc.*, 2010, **132**, 3270; (b) H. Wang, H. S. Casalongue, Y. Liang and H. Dai, *J. Am. Chem. Soc.*, 2010, **132**, 7472; (c) W. Zhou, X. Cao, Z. Zeng, W. Shi, Y. Zhu, Q. Yan, H. Liu, J. Wang and H. Zhang, *Energy Environ. Sci.*, 2013, **6**, 2216; (d) Z. Yin, J. Zhu, Q. He, X. Cao, C. Tan, H. Chen, Q. Yan and H. Zhang, *Adv. Energy Mater.*, 2014, **4**, 1300574; (e) X. Cao, Z. Yin and H. Zhang, *Energy Environ. Sci.*, 2014, **7**, 1850; (f) J. Zhu, D. Yang, Z. Yin, Q. Yan and H. Zhang, *Small*, 2014, DOI: 10.1002/smll.201303202.
18. (a) S. Gan, L. Zhong, T. Wu, D. Han, J. Zhang, J. Ulstrup, Q. Chi and L. Niu, *Adv. Mater.*, 2012, **24**, 3958; (b) N. Zhu, S. Han, S. Gan, J. Ulstrup and Q. Chi, *Adv. Funct. Mater.*, 2013, **23,** 5297.
19. W. E. Ford, *J. Photochem.*, 1987, **37**, 189.

20. D. R. Dreyer, S. Park, C. W. Bielawski and R. S. Ruoff, *Chem. Soc. Rev.*, 2010, **39**, 228.
21. M. Chen, L. Hu, J. Xu, M. Liao, L. Wu and X. Fang, *Small*, 2011, **7**, 2449.
22. L. Hu, L. Wu, M. Liao and X. Fang, *Adv. Mater.*, 2011, **23**, 1988.
23. P. V. Kamat, K. Tvrdy, D. R. Baker and J. G. Radich, *Chem. Rev.*, 2010, **110**, 6664.
24. A. Wojcik and P. V. Kamat, *ACS Nano*, 2010, **4**, 6697.
25. (a) J. Malig, N. Jux and D. M. Guldi, *Acc.Chem. Res.*, 2013, **46**, 53-64. (b) K. Dirian, M. Angeles Herranz, G. Katsukis, J. Malig, L. Rodriguez-Perez, C. Romero-Nieto, V. Strauss, N. Martin and D. M. Guldi, *Chem. Sci.*, 2013, **4**, 4335-4353. (c) J. Malig, N. Jux, D. Kiessling, J.-J. Cid, P. Vazquez, T. Torres and D. M. Guldi, *Angew. Chem. Int. Ed.*, 2011, **50**, 3561-3565. (d) M.-E. Ragoussi, J. Malig, G. Katsukis, B. Butz, E. Spiecker, G. de la Torre, T. Torres and D. M. Guldi, *Angew. Chem. Int. Ed.*, 2012, **51**, 6421-6425.
26. (a) A. Hirsch, J. M. Englert and F. Hauke, *Acc. Chem. Res.*, 2013, **46**, 87-96. (b) J. M. Englert, J. Rohrl, C. D. Schmidt, R. Graupner, M. Hundhausen, F. Hauke and A. Hirsch, *Adv. Mater.*, 2009, **21**, 4265; (c) N. V. Kozhemyakina, J. M. Englert, G. A. Yang, E. Spiecker, C. D. Schmidt, F. Hauke and A. Hirsch, *Adv. Mater.*, 2010, **22**, 5483; (d) C. Backes, F. Hauke and A. Hirsch, *Adv. Mater.*, 2011, **23**, 2588.
27. D. M. Eisele, J. Knoester, S. Kirstein, J. P. Rabe and D. A. Vanden Bout, *Nat. Nanotech.*, 2009, **4**, 658.

